ResearchGate

See discussions, stats, and author profiles for this publication at: https://www.researchgate.net/publication/299496735

Naphthodithieno[3,2-b]thiophene-based donor-acceptor copolymers: Synthesis, characterization, and their photovoltaic...

Article *in* Dyes and Pigments · March 2016

DOI: 10.1016/j.dyepig.2016.03.048

CITATIONS
2

READS
61

11 authors, including:

Weifeng Zhang
Chinese Academy of Sciences
53 PUBLICATIONS **401** CITATIONS
SEE PROFILE

Weilong Zhou
Jilin University
10 PUBLICATIONS **45** CITATIONS
SEE PROFILE

Fenghong Li
Jilin University
60 PUBLICATIONS **1,785** CITATIONS
SEE PROFILE

Weiping Wu
University of Cambridge
184 PUBLICATIONS **5,155** CITATIONS
SEE PROFILE

Some of the authors of this publication are also working on these related projects:

conjugated materials and magnetic properties View project

DSSC solar cells and perovskite solar cells View project

All content following this page was uploaded by Weifeng Zhang on 06 April 2016.

The user has requested enhancement of the downloaded file.

Dyes and Pigments 131 (2016) 1–8

Contents lists available at ScienceDirect

Dyes and Pigments

journal homepage: www.elsevier.com/locate/dyepig

Naphthodithieno[3,2-*b*]thiophene-based donor-acceptor copolymers: Synthesis, characterization, and their photovoltaic and charge transport properties

Weifeng Zhang [a], Keli Shi [a], Weilong Zhou [b], Zhaoguang Li [c], Zhihui Chen [a], Jie Xu [a], Donghang Yan [d], Yanchun Han [d], Man Shing Wong [c, ***], Fenghong Li [b, **], Gui Yu [a, *]

[a] Beijing National Laboratory for Molecular Sciences, Institute of Chemistry, Chinese Academy of Sciences, Beijing 100190, PR China
[b] State Key Laboratory of Supramolecular Structure and Materials, Jilin University, Changchun 130012, PR China
[c] Institute of Molecular Functional Materials, Department of Chemistry and Institute of Advanced Materials, Hong Kong Baptist University, Kowloon Tong, Hong Kong SAR, PR China
[d] State Key Laboratory of Polymer Physics and Chemistry, Changchun Institute of Applied Chemistry, Chinese Academy of Sciences, Changchun 130022, PR China

ARTICLE INFO

Article history:
Received 2 February 2016
Received in revised form
25 March 2016
Accepted 26 March 2016
Available online 29 March 2016

Keywords:
Naphthodithieno[3,2-*b*]thiophenes
Isoindigos
Copolymers
Photovoltaic properties
Charge transport properties

ABSTRACT

Herein, we report the synthesis, characterization, and their photovoltaic and field−effect properties of two dialkoxyl-substituted naphthodithieno[3,2-*b*]thiophene (**NDTT**)-based copolymers, namely **P1** and **P2**. The NDTT-based copolymers exhibit broad absorption profiles throughout the visible spectrum up to ca. 800 nm. The copolymers have HOMO/LUMO energy levels of ca. −5.14 eV/−3.52 eV. The dialkoxyl-substituted NDTT units endow the copolymers with enhanced solution processability, and crystalline stacking thin films with small π−π distances of down to 3.59 Å. Polymer-fullerene bulk heterojunction solar cells that fabricated from a blend of **P2**/$PC_{71}BM$ using diiodooctane as a solvent additive, afforded the highest power conversion efficiency of 3.54%. Solution-processed polymer field-effect transistors based on **P1** with bottom-gate bottom-contact geometry exhibited promising hole mobilities of 0.070 $cm^2\ V^{-1}\ s^{-1}$.

© 2016 Elsevier Ltd. All rights reserved.

1. Introduction

Due to the merits of low cost, solution processability, lightweight, and flexibility, as well as the strong urge for renewable energy sources, organic electronics has become one of the frontier research areas during the past decades [1,2]. Efficiently harvesting solar energy by organic photovoltaic (OPV) cells and achieving high charge carrier transport in organic field-effect transistors (OFETs) are the ultimate goals of the relating academic and industrial research circles [3–6]. In the regard, donor-acceptor (D–A) polymer-fullerene bulk heterojunction solar cells, which are the most successful OPV devices with a bicontinuous interpenetrating network of electron donor and acceptor materials, have been developed significantly [7–9]. Their power conversion efficiencies (PCEs) have reached over 10% in a single junction solar cell [10]. Meanwhile, solution-processed polymer field-effect transistors (PFETs) have also achieved great progress in recent years [11,12]. However, the PCEs and charge carrier mobilities of polymer semiconductors still lag behind those of inorganic counterparts. Hence, further development of new polymer conjugated systems and π-extended building blocks and understanding structure−property relationships are of great necessary for simultaneously obtaining good physical and functional properties, including high thermal stability, broad and intense photoabsorption, prompt charge separation, and efficient charge transport.

In past decades, many thienoacene-based building blocks were designed and applied in constructing D–A copolymers due to their outstanding performance in small-molecule organic semiconductors [13,14]. Among them, the benzodithiophene-based copolymers often exhibited high charge carrier mobilities or PCEs. Planar fused-ring thienoacene-based building blocks with large π-conjugated systems were anticipated to be more beneficial for

* Corresponding author.
** Corresponding author.
*** Corresponding author.
E-mail addresses: mswong@hkbu.edu.hk (M.S. Wong), fhli@jlu.edu.cn (F. Li), yugui@iccas.ac.cn (G. Yu).

http://dx.doi.org/10.1016/j.dyepig.2016.03.048
0143-7208/© 2016 Elsevier Ltd. All rights reserved.

constructing high-performance polymer semiconductors for OFETs because larger and more planar conjugated backbones are easier to acquire enlarged overlapping areas between π-orbitals, which enhanced the charge carrier mobility [15]. However, the kind of thienoacene-based building blocks has seldom been successful in developing high-performance polymer semiconductors due to their too rigid structures and/or the inconvenience of introducing alkyl groups, which lead to the resulting polymers with low solution processability. To overcome these difficulties, many fused-ring thienoacene-based building blocks and organic semiconductors had been developed. For example, Liu et al. synthesized series of novel soluble fused-ring thienoacene-based small-molecule and polymer materials and applied in OFET devices [16]. Our group developed series of naphtho[2,1-*b*:3,4-*b*′]dithiophene-based organic semiconductors, and investigated their photovoltaic and field−effect properties [17]. Yang and coworkers also synthesized alternating polymer, naphtha[2,1-*b*:3,4-*b*′]dithiophene-4,7-di(thiophen-2-yl) -benzothiadiazole (PNDT-DTB), which afforded PCE of 3.36% through optimizing alkyl side chains [18]. More recently, our group synthesized a series of π-extended naphthodithieno[3,2-*b*]thiophene (**NDTT**)-based small molecules, which exhibited promising mobilities of up to 0.22 $cm^2 V^{-1} s^{-1}$ [19]. The **NDTT$_S$** possess alkylated planar 6-fused-ring structure and own the HOMO energy levels of ca. −5.18 eV, implying that they have great potential in developing air-stable polymer semiconductors.

In this work, we report the synthesis, characterization and their photovoltaic and field−effect properties of two **NDTT**-based D−A copolymers, namely **P1** and **P2**, in which alkylated isoindigo moiety is adopted as an acceptor unit. The two copolymers exhibit broad absorption throughout the visible spectrum up to ca. 800 nm in solutions and thin films, suggesting that effective intermolecular and intramolecular interactions occur between the donor and acceptor units, and the **NDTTs** have strong electron-donating property. Moreover, the **NDTT** units endow the two copolymers with enhanced solution processability, and ordered and crystalline thin films with close packing mode with small π−π stacking distances of down to 3.59 Å, which is thought to be favorable for charge carrier transport. As a result, the PSCs based on **P1** and **P2** afforded promising PCE of up to 3.54%. While the **P1** and **P2**-based PFETs exhibit the highest hole mobilities of 0.070 and 0.040 $cm^2 V^{-1} s^{-1}$, respectively. These results demonstrate that the dialkoxyl-substituted **NDTT** units are a kind of potential building blocks in constructing D−A polymer semiconductors for organic electronics.

2. Experimental section

2.1. Materials and instruments

All chemicals were purchased from commercial sources and used without further purification unless otherwise noted. 6,6′-Dibromo-*N*,*N*′-(2-octyldodecanyl)-isoindigo, **6** was synthesized according to the method reported [20]. Tetrahydrofuran (THF) was dried by sodium/benzophenone, and freshly distilled before use under Ar.

NMR spectra were collected on a Bruker-300 NMR spectrometer in $CDCl_3$, and the chemical shifts were referenced to TMS (0 ppm) and $CDCl_3$ (77 ppm), respectively. Mass spectra and elemental analyses were carried on a Waters Micromass GCT spectrometer and CARLO ERBA 1106 Elemental Analyzer, respectively. Thermogravimetric analyses were performed on a Perkin−Elmer series 7 thermal analysis system under N_2 at a heating rate of 10 °C min^{-1}. The copolymer thin films for UV−Vis absorption spectra measurements were fabricated by spin coating of a copolymer solution in chlorobenzene onto quartz substrate. UV−Vis absorption spectra were measured using a Hitachi U-3010 spectrophotometer. The electrochemical properties of the copolymers were investigated using cyclic voltammetry workstation (CHI660A) with a standard three-electrode electrochemical cell in N_2-saturated solution of 0.1 M Bu_4NPF_6 in dry acetonitrile. Platinum stick, Ag/AgCl, and platinum wire were used as the working electrode, reference electrode, and counter electrode, respectively. High temperature gel permeation chromatography (GPC) measurements were carried out on a Polymer Labs PL 220 system using a refractive index detector at 150 °C with 1,2,4-trichlorobenzene as the eluent and polystyrenes as standards.

2.2. Fabrication and characterization of PSCs

All PSCs were fabricated with a device configuration of ITO/PEDOT:PSS/copolymers:$PC_{71}BM$([6,6]-phenyl-C_{71}-butyric acid methyl ester)/poly[(9,9-bis(3′-(*N*,*N*-dimethylamino)propyl) −2,7-fluorene)-alt-2,7-(9,9-dioctyl fluorene)](PFN)/Al. The ITO-coated glass substrates (15Ω/□) were ultrasonically cleaned sequentially in deionized water, acetone, and ethanol, and treated by UV/O_3 for 20 min. The PEDOT:PSS layer was fabricated by spin-coating onto the ITO substrate at 3500 rpm for 1 min, followed by thermally annealing at 110 °C for 30 min. For regular devices, the copolymer:$PC_{71}BM$ active layer (20 mg mL^{-1}) was spin-coated from a mixed solvent of *o*-dichlorobenzene:1,8-diiodoctane (97:3 vol %) at 1000 rpm for 1 min, and then annealed at room temperature in a vacuum oven for 12 h. The thickness of the resulting film was measured with a Dektak III surface profilometer. PFN dissolved in methanol (2 mg mL^{-1}) containing a small amount of AcOH was spin-coated on the active layer. Finally, Al (100 nm) was successively deposited as a cathode by thermal evaporation under high vacuum through a shadow mask. All devices have an active area of 2 × 2 mm^2. Current density−voltage characteristics were recorded using a computer-controlled Keithley 2400 Source Meter under AM 1.5 illumination with an intensity of 100 mW cm^{-2} in a N_2 glove box. External quantum efficiency spectra of the encapsulated PSCs were characterized using Q Test Station 2000 (Crowntech Inc. USA). AFM images were measured with an S II Nanonaviprobe station 300 HV (Seiko, Japan) in contact modes.

2.3. Fabrication and characterization of PFETs

All PFETs with bottom-gate bottom-contact (BGBC) configuration were fabricated on n^{++}-Si/SiO_2 (300 nm) substrates, in which n^{++}-Si and SiO_2 were used as the gate electrode and gate dielectric, respectively, and Gold/titanium (30 nm/5 nm) was adopted as source/drain electrodes. Prior to device fabrication, the n^{++}-Si/SiO_2 substrates were cleaned sequentially in acetone, ethanol, deionized water, and isopropanol, and then treated with plasma for 15 min and modified with an octadecyltrichlorosilane (OTS) self-assembled monolayer. The copolymers were fabricated by spin coating of a polymer solution (10 mg mL^{-1}) in dichlorobenzene, optionally followed by a thermal annealing for 5 min. Thin film morphologies were studied on a Digital Instruments Nanoscope V atomic force microscope operated in tapping modes, and GXRD illuminated at a constant incidence angle of 0.2°. The output and transfer characteristics of the PFET devices were determined on a Keithley 4200 parameter analyzer. Both fabricating and measuring process were performed under ambient conditions. The carrier mobility, μ, was calculated from the data in the saturated regime according to the equation,

$$I_{DS} = \left(\frac{W}{2L}\right) C_i \mu (V_G - V_T)^2$$

where I_{DS} is the saturation drain current, W/L is the channel width/length, C_i is the capacitance per unit area of the gate dielectric layer, and V_G and V_T are the gate voltage and threshold voltage, respectively.

2.4. Synthesis

2.4.1. 3,10-Ditrimethylstannyl-6,7-didecyloxynaphthodithieno[3,2-b]thiophene (**5a**)

To an Ar-saturated flask containing **4a** (133 mg, 0.20 mmol) and THF (10 mL) were added dropwise 2.5 M of *n*-BuLi (0.20 mL, 0.50 mmol) at −78 °C. The resultant solution was stirred at the same temperature for 1 h, and then slowly warmed to 0 °C and maintained for 5 min. After cooled to −78 °C again, 1.0 M of trimethylin chloride (0.50 mL, 0.50 mmol) was added in one portion. The reaction system was warmed to room temperature and stirred for overnight. After quenched with saturated NH_4Cl (aq.), the reaction mixture was extracted with diethyl ether, followed by dried over Na_2SO_4. After removal of the solvents under reduced pressure, the solid residue was recrystallized from hexane affording the title compound as a white solid (125 mg, 63%). ^{1}H NMR (300 MHz, $CDCl_3$) δ: 7.93 (s, 2H), 7.48 (s, 2H), 4.38 (t, J = 6.6 Hz, 4H), 2.06–1.99 (m, 4H), 1.67–1.59 (m, 4H), 1.46–1.28 (m, 24H), 0.90–0.85 (m, 6H), 0.50 (s, 18H). ^{13}C NMR (75 MHz, $CDCl_3$) δ: 148.9, 141.7, 140.8, 138.2, 133.9, 127.2, 126.2, 121.6, 106.9, 69.3, 31.9, 29.8, 29.7, 29.6, 29.4, 29.2, 26.3, 22.7, 14.1, −7.9. HRMS (MALDI-TOF): calcd for $C_{44}H_{64}O_2S_4Sn_2$: 990.1836; found: 990.1833.

2.4.2. 3,10-Ditrimethylstannyl-6,7-didodecyloxynaphthodithieno[3,2-b]thiophene (**5b**)

The synthetic procedure of **4a** was followed using **4b** (130 mg, 0.18 mmol) affording the title compound as a white solid (126 mg, 67%). ^{1}H NMR (300 MHz, $CDCl_3$) δ: 7.94 (s, 2H), 7.49 (s, 2H), 4.38 (t, J = 6.6 Hz, 4H), 2.06–1.99 (m, 4H), 1.67–1.59 (m, 4H), 1.46–1.27 (m, 32H), 0.90–0.85 (m, 6H), 0.50 (s, 18H). ^{13}C NMR (75 MHz, $CDCl_3$) δ: 148.9, 141.7, 140.8, 138.2, 133.9, 127.2, 126.2, 121.6, 106.9, 69.3, 31.9, 29.8, 29.7, 29.6, 29.4, 29.2, 22.7, 14.1, −7.9. HRMS (MALDI-TOF): calcd. for $C_{48}H_{72}O_2S_4Sn_2$: 1046.2463; found: 1046.2464.

2.4.3. General procedures for stille polymerization and polymer purification

An Ar-saturated Schlenk tube containing **6** (0.10 mmol), **5a** or **5b** (0.10 mmol), $Pd_2(dba)_3$ (5.0 mg), P(*o*-toyl)$_3$ (12 mg), and chlorobenzene (5.0 mL) was heated to 110 °C and stirred for 24 h. After cooling down to room temperature, the reaction mixture was poured into 100 mL of methanol containing 2 mL of hydrochloric acid and stirred for 2 h. The resulting blue-purple crude polymer was collected by filtration and subjected to Soxhlet extraction for 2 days in methanol, acetone, and hexane for the removal of the low-molecular-weight fraction of the material and residual catalytic impurities. The residue was finally collected with chlorobenzene to obtain the target polymers.

P1: (137 mg, 92%).^{1}H NMR (300 MHz, $C_2D_2Cl_4$) δ: 9.22–9.00 (br, 2H), 8.14–7.90 (br, 2H), 7.72–7.28 (br, 4H), 4.91–4.27 (br, 4H), 3.87–3.58 (br, 4H), 2.36–1.02 (br, 96H). Elemental anal. calcd. for $C_{94}H_{136}N_2O_4S_4$: C, 75.96; H, 9.22; N, 1.88; Found: C 76.35, H 9.05, N 1.76.

P2: (140 mg, 90%). ^{1}H NMR (300 MHz, $C_2D_2Cl_4$) δ: 9.20–8.94 (br, 2H), 8.22–7.83 (br, 2H), 7.70–7.24 (br, 4H), 4.86–4.19 (br, 4H), 3.85–3.53 (br, 4H), 2.33–1.00 (br, 104H). Elemental anal. calcd. for $C_{98}H_{144}N_2O_4S_4$: C, 76.31; H, 9.41; N, 1.82; Found: C 75.63, H 9.24, N 1.79.

3. Results and discussion

3.1. Synthesis and thermal properties

The chemical structures and synthetic routes of **P1** and **P2** are shown in Scheme 1. Naphthodithieno[3,2-*b*]thiophenes, **4a** and **4b**, were synthesized according to the methods reported [19]. The key intermediates **5a** and **5b** were converted from **4a** and **4b** in a standard synthetic procedure, respectively. Stille-coupling polymerization of **5a** or **5b**, and **6** were carried out in the presence of $Pd_2(dba)_3$ and P(*o*-tol)$_3$ as catalysts affording respective crude copolymers as purple solids. These crude products were further purified by Sohxlet extraction to remove the residual catalytic metal and low-molecular-weight oligomers, giving the desired polymers as purple films in excellent yields of 90–92%. The copolymers have good solubility in common solvents such as chloroform and chlorobenzene. High temperature GPC measurements show that the number-average molecular weights (M_n), the weight-average molecular weights (M_w), and polydispersity indexes (PDI) are 23.7, 69.5 *kDa*, 2.93 for **P1**, and 24.7, 71.9 *kDa*, 2.90 for **P2**, respectively. Thermogravimetric analyses (TGA) demonstrate that the decomposition temperatures (T_{dec}) with 5% weight loss for the two polymers are both higher than 380 °C, indicating that both copolymers have good thermal stability (Fig. 1a, Table 1).

3.2. Optical and electrochemical properties

Fig. 1b shows the UV–Vis absorption spectra of the copolymers in the chlorobenzene solutions and thin films, and the optical data are summarized in Table 1. The two copolymers exhibit similar absorption spectra in solutions due to the same π-conjugated backbone. Both absorption profiles are composed of two characteristic absorption bands. The weak band ranging from 350 to 480 nm with peak at ca. 425 nm is associated with high energy π–π* transitions [6b], while the intense, broad one ranging from 500 to 780 nm with peak at ca. 720 nm is attributed to strong intramolecular charge transfer between the II units and **NDTT** units [21]. Compared to in solutions, the thin films show broader and red-shifted absorption spectra, meaning that aggregation or orderly packing occurs in thin films [22]. On the basis of thin film absorption cutoff values of 788 and 798 nm, the optical bandgaps (E_g^{opt}) of **P1** and **P2** were estimated to be 1.57 and 1.56 eV, respectively. It is well-recognized that the frontier orbital energy levels are critical to the functioning of PSC and PFET devices, so the electrochemical properties of copolymers were also evaluated with cyclic voltammetry (CV). As shown in Fig. 2a, the onset oxidation potentials (E_{onset}^{ox}) of **P1** and **P2** are 0.74 and 0.77 V, thus their HOMO energy levels could be estimated to be −5.14 and −5.17 eV, respectively, calculated from the equation of HOMO = −(4.4+E_{onset}^{ox}) [23]. The LUMO energy levels were calculated from the difference between the HOMO energy levels and E_g^{opt} values as −3.57 eV for **P1** and −3.61 eV for **P2**. As the HOMO energy levels are close to the work function of Au electrode, it would also facilitate hole injection from gold electrodes to the copolymer thin films (Fig. 2b).

3.3. Photovoltaic properties

PSCs using **P1** and **P2** as the donors and $PC_{71}BM$ as the acceptors were fabricated with the conventional device configuration of ITO/PEDOT:PSS/copolymer: $PC_{71}BM$/PFN/Al. Photovoltaic properties of the PSCs were measured under AM 1.5 simulated solar illumination at an irradiation intensity of 100 mW cm^{-2}. The **P1**- and **P2**-based PSCs exhibit the highest PCE of 3.18 and 3.54%, respectively (Fig. S1).

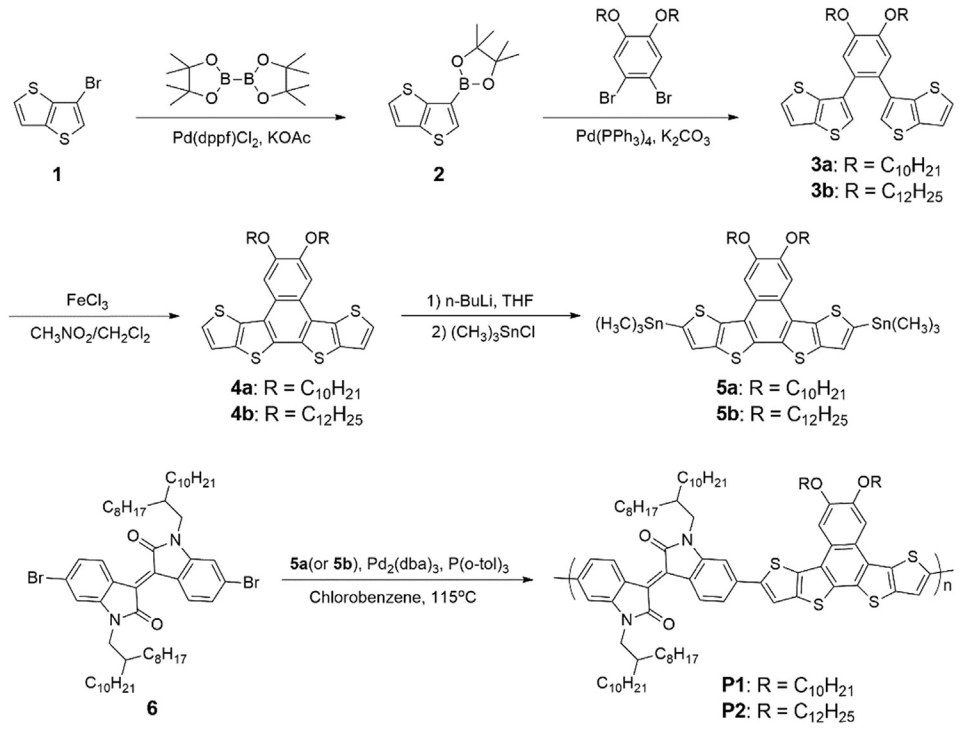

Scheme 1. The chemical structures and synthetic routes of **P1** and **P2**.

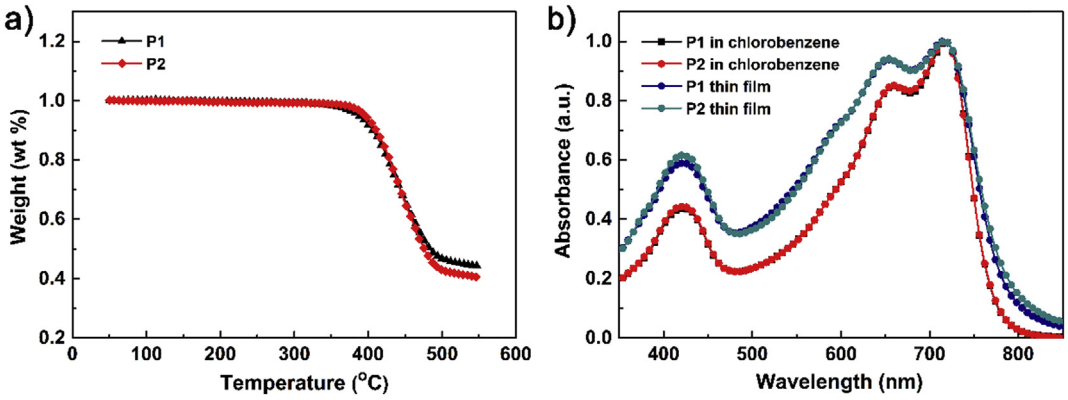

Fig. 1. (a) TGA traces of **P1** and **P2**. (b) UV–Vis absorption spectra of **P1** and **P2** in chlorobenzene solutions and thin films.

Table 1
Molecular weights, thermal, photophysical and electrochemical properties of **P1** and **P2**.

Copolymer	M_n[a] (*kDa*)	M_w[a] (*kDa*)	*PDI*[a]	T_{dec}[b] (°C)	λ_{max}	E_g^{opt} (eV)	E_{onset}^{ox} (V)[e]	HOMO (eV)[e]	LUMO (eV)[f]
P1	23.7	69.5	2.90	380	680[c]/670[d]	1.57	0.74	−5.14	−3.57
P2	24.7	71.9	2.93	392	670[c]/670[d]	1.56	0.77	−5.17	−3.61

[a] Determined by GPC at 150 °C.
[b] Measured by TGA.
[c] In chlorobenzene solutions.
[d] Thin films.
[e] Determined by CV. HOMO = $-(4.4 + E_{onset}^{ox})$ eV.
[f] LUMO = (HOMO + E_g^{opt}) eV.

It can be found that the device performance is sensitive to the treatments with 1,8-diiodooctane (DIO) as a solvent additive (Table S1). For the PSCs that fabricated from the blend of **P1** and $PC_{71}BM$ in *o*-dichlorobenzene:DIO (97:3 vol%), the open-circuit voltage (V_{oc}), short circuit current (J_{sc}) and fill factor (*FF*) are 0.79 V, 6.87 mA cm^{-2}, and 0.57, respectively. The corresponding PCE is 3.12%. Whereas, the V_{oc} of 0.78 V, the J_{sc} of 5.92 mA cm^{-2}, the *FF* of 0.60, and the PCE of 2.74% are obtained without DIO. Obviously, the addition of DIO facilitates to form continuous and homogeneous morphology, thus affords the improved PCE [21].

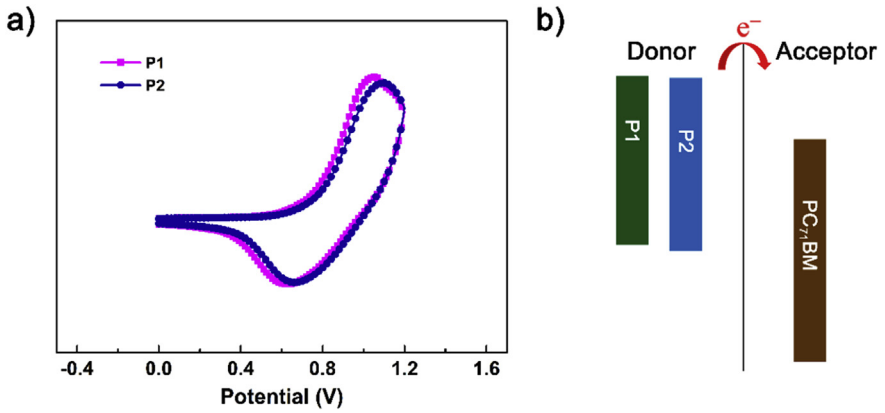

Fig. 2. (a) CV traces of **P1** and **P2**. (b) Energy level diagrams for **P1** and **P2** as donors and $PC_{71}BM$ as the acceptor.

Table 2
Summary of the optimized PSC and PFET device performances.

Copolymer	J_{sc}[a] (mA cm^{-2})	V_{oc}[a] (V)	FF[a] (%)	PCE[a] (%)	μ[b] (cm^2 V^{-1} s^{-1})	I_{on}/I_{off}[b,d]	V_{th}[b,e] (V)
P1	6.92	0.785	59	3.18	0.070	1.2×10^3	0
P2	7.95	0.785	56	3.51	0.040[c]	4.0×10^2	−6

[a] Device configuration: ITO/PEDOT:PSS (35 nm)/copolymer:$PC_{71}BM$(1:2)/PFN(3 nm)/Al (100 nm) using 3 vol% of DIO as a solvent additive.
[b] BGBC configuration after thermal annealing at 120 °C.
[c] After thermal annealing at 160 °C.
[d] I_{on}/I_{off} refers to the on-to-off ratio.
[e] Refers to the threshold voltage.

Table 2 presents a summary of J_{sc}, V_{oc}, *FF*, and PCE of the PSCs based on **P1**/**P2**: $PC_{71}BM$ = 1:2 using 3 vol% of DIO. It is clear that the PSC based on **P2** displays higher PCE due to higher J_{sc} and slightly higher *FF* than the counterpart based on **P1**. However, the two devices have the same V_{oc} due to similar HOMO levels of **P1** and **P2**.

To obtain higher device performance, the ratio of **P2**: $PC_{71}BM$ was further tuned from 1:1.5 (60 wt% for $PC_{71}BM$), 1:2 (67 wt% for $PC_{71}BM$), to 2:5 (71 wt% for $PC_{71}BM$). Fig. 3a presents current density-voltage (*J-V*) characteristics of the three devices with **P2**: $PC_{71}BM$ ratios from 1:1.5 to 1:2.5 under illumination, and the device performance parameters are summarized in Table 3. Apparently, the V_{oc} values slightly decrease from 0.775 V to 0.770 V with the $PC_{71}BM$ weight fraction changing from 60% to 71%. This trend is consistent with previous results in other systems observed by Veldman *et. al* [24]. The device with **P2**: $PC_{71}BM$ ratios (1:2) exhibit the highest PCE (3.54%) due to the highest J_{sc} of 7.21 mA cm^{-2} and *FF* of 63.7% among the three devices. The external quantum efficiency (EQE) of the PSCs were measured under monochromatic light. Fig. 3b illustrates the three devices have broad photo responses ranging from 380 to ca. 800 nm, which is consistent with the UV–Vis absorption spectra of the **P2** thin film as demonstrated in Fig. 2b. The J_{sc}-EQE value of device with **P2**: $PC_{71}BM$ ratios (1:2) is 7.11 mA cm^{-2}, which is in good agreement with J_{sc} of 7.21 mA cm^{-2} (ca. 1.4% error) obtained from *J–V* characteristics under illumination. The finding indicates that the J_{sc} value measured for the PSCs is reliable and the PCE value is not overvalued. In addition, the device with **P2**: $PC_{71}BM$ ratios (1:2) has the lowest series resistance (R_s) and the highest shunt resistance (R_{sh}) in the devices. We propose that the lower R_s (13.6 Ω cm^2) and higher R_{sh} (1451 Ω cm^2) of **P2**:$PC_{71}BM$ (1:2) film result in higher J_{sc} and *FF* due to its high-quality uniform morphology as observed in AFM images (Fig. S2).

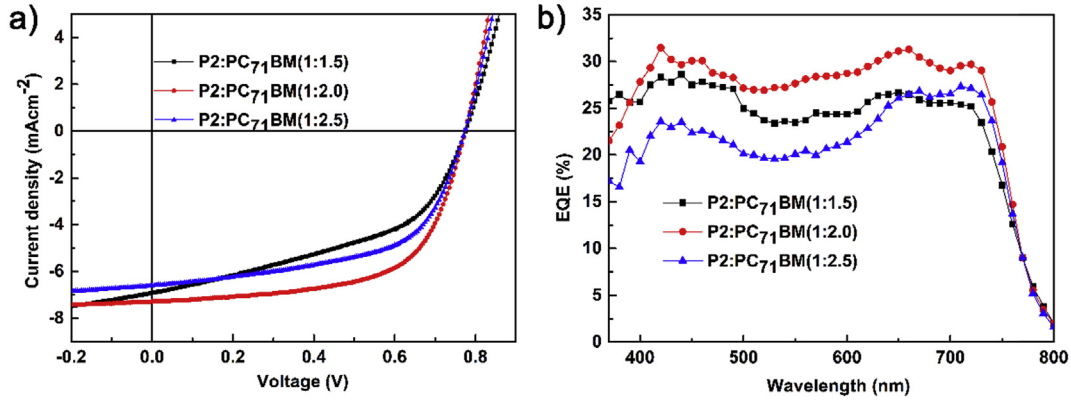

Fig. 3. (a) The current density–voltage (*J–V*) curves and (b) The external quantum efficiency (EQE) spectra of PSCs fabricated based on **P2**:$PC_{71}BM$.

Table 3
The performances of the PSCs based on various **P2**: $PC_{71}BM$ ratio.

Donor: Acceptor	PCE (%)	J_{sc} (mA cm^{-2})	V_{oc} (V)	*FF* (%)	J_{sc}-EQE (mA cm^{-2})	R_s (Ω cm^2)	R_{sh} (Ω cm^2)
1:1.5	2.51	7.00	0.775	0.464	6.34	19.9	526
1:2.0	3.54	7.21	0.770	0.637	7.11	13.6	1451
1:2.5	2.95	6.53	0.770	0.587	5.72	16.1	975

3.4. Field–effect properties

The charge transport properties of the two copolymers were investigated by fabricating PFETs with bottom-gate bottom-contact structures. The fabricating, annealing, and measuring processes were all carried out in ambient conditions. As anticipated, both copolymers exhibit typical *p*-type charge transport characteristics. The typical output (I_{DS}–V_{DS}) and transfer (I_{DS}–V_{GS}) curves of PFET based on **P1** and **P2** are shown in Fig. 4, and the resulting parameters are summarized in Table 2. The pristine film of **P1** exhibit hole mobility of 0.017 cm^2 V^{-1} s^{-1} with an on/off current ratio of 8.80×10^5, while the annealed film (at 120 °C for 5 min) showed an improved hole mobility of 0.025 cm^2 V^{-1} s^{-1} with an on/off current ratio of 1.5×10^6, and even the highest mobility of 0.070 cm^2 V^{-1} s^{-1}. As the annealing temperature elevated from 80 to 200 °C, the mobility of **P1** thin film has gone through a process of a progressive increase followed by a progressive decrease (Tables S2). The reason could be attributed to that the morphology/molecular packing in thin films become more ordered in the initial stage with the annealing temperature increasing. However, once beyond an optimal temperature, the discontinuities in the film create with an increase in intergranular spaces when the grain size becomes very large. The discontinuous polymer domains result in trapping of charge carriers [25]. The pristine film of **P2** afford a hole mobility of 0.014 cm^2 V^{-1} s^{-1} with an on/off current ratio of 1.70×10^5, while the annealed film demonstrate hole mobility of 0.028 cm^2 V^{-1} s^{-1} with an on/off current ratio of 3.1×10^5, and even the highest mobility of 0.040 cm^2 V^{-1} s^{-1}. A similar mobility change

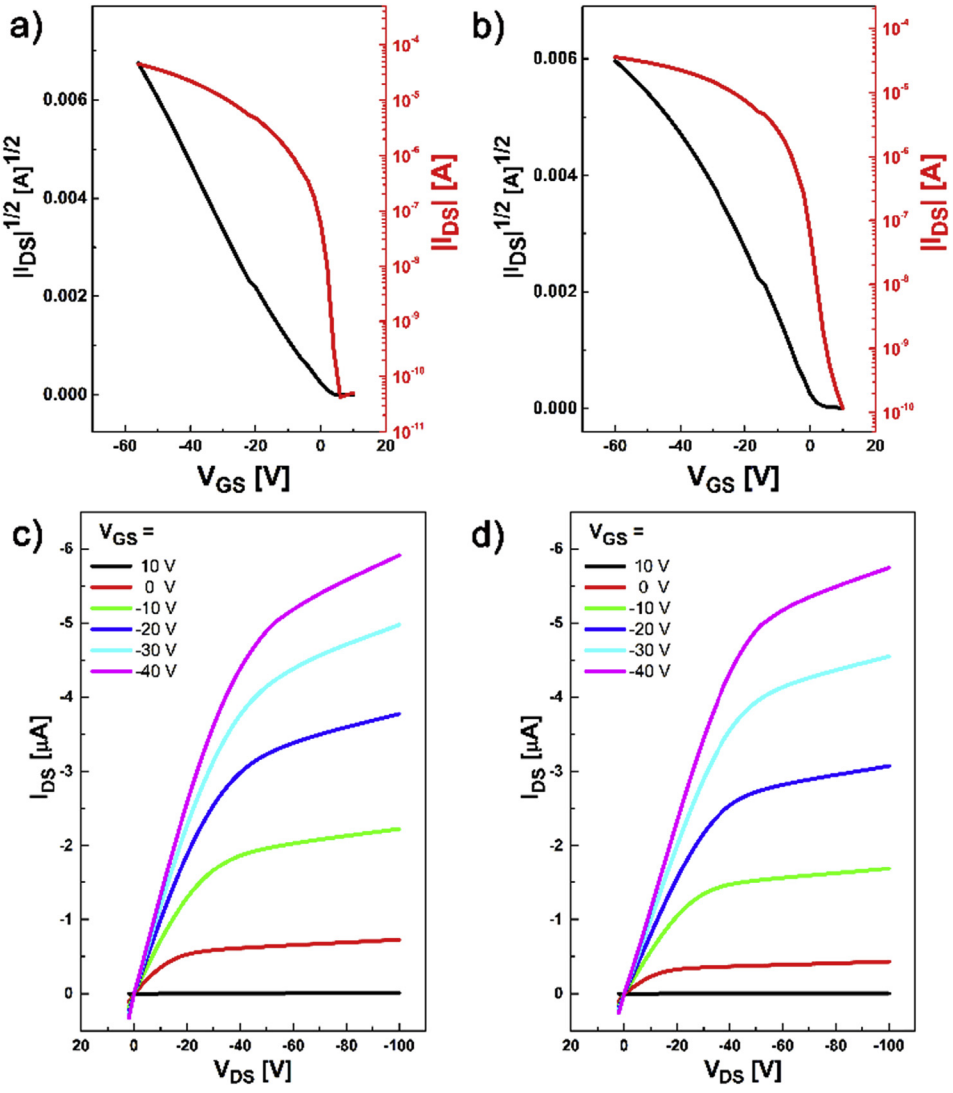

Fig. 4. Typical *p*-type (a) output and (b) transfer characteristics of the PFETs based on the copolymers: a), c) **P1**; b), d) **P2**.

is also observed in **P2** thin films with the annealing temperature increasing from 80 to 200 °C.

3.5. Thin film microstructure investigations

For better understanding the correlation between material structure and PFET performance, AFM and GXRD were employed to investigate the microstructures of **P1** and **P2** thin films. As shown in Fig. 5a, b, and Fig. S2, both copolymers form uniform thin films with clear crystalline zones both in the pristine and annealed films. In the annealed films, however, the crystalline grains are smaller and the grain boundaries are fewer than those in the pristine films. The dense and crystalline thin film morphology is more favorable for charge carrier transport [11]. Fig. 5c and d presents the GXRD patterns of **P1** and **P2** thin films before and after annealing including out-of-plane and in-plane orientations. These thin films all show lamellar texture judged by the apparent (*h*00) Bragg peaks in out-of-plane patterns. The (*h*00) Bragg peaks of the annealed films of **P1** and **P2** corresponding to (100), (200), and (300) are all stronger and sharper than the corresponding counterpart in their pristine films. Especially, the 2θ of the (100) Bragg peak for **P1** shifts from 3.50° to 3.70° before and after annealing, respectively. On the basis of the 2θ values, the *d*–*d* spacing distances were estimated to be 25.36 Å for the pristine film and 23.99 Å for the annealed film, respectively. The observations suggest that the annealed **P1** thin film has improved crystallinity [26]. Moreover, the (010) Bragg peak of the annealed **P1** film related to π–π stacking is stronger than that of the pristine film. Based on the 2θ of 25°, the π–π stacking distance of the **P1** films was estimated to be of 3.59 Å. A similar change trend in molecular packing was observed in the **P2** films before and after annealing. The AFM images and GXRD patterns indicate that the annealed films of both copolymers own slightly dense, enhanced molecular packing, and improved crystallinity, which match well with the changes in mobility as aforementioned.

4. Conclusions

In summary, we have synthesized and characterized two dialkoxyl-substituted naphthodithieno[3,2-*b*]thiophene (**NDTT**)-based copolymers, and investigated their semiconducting properties by fabricating photovoltaic cells and field-effect transistors. The dialkoxyl-substituted NDTT units endow the copolymers with broad absorption profile, enhanced solution processability, and crystalline stacking with small π–π distance in thin films. PSCs and

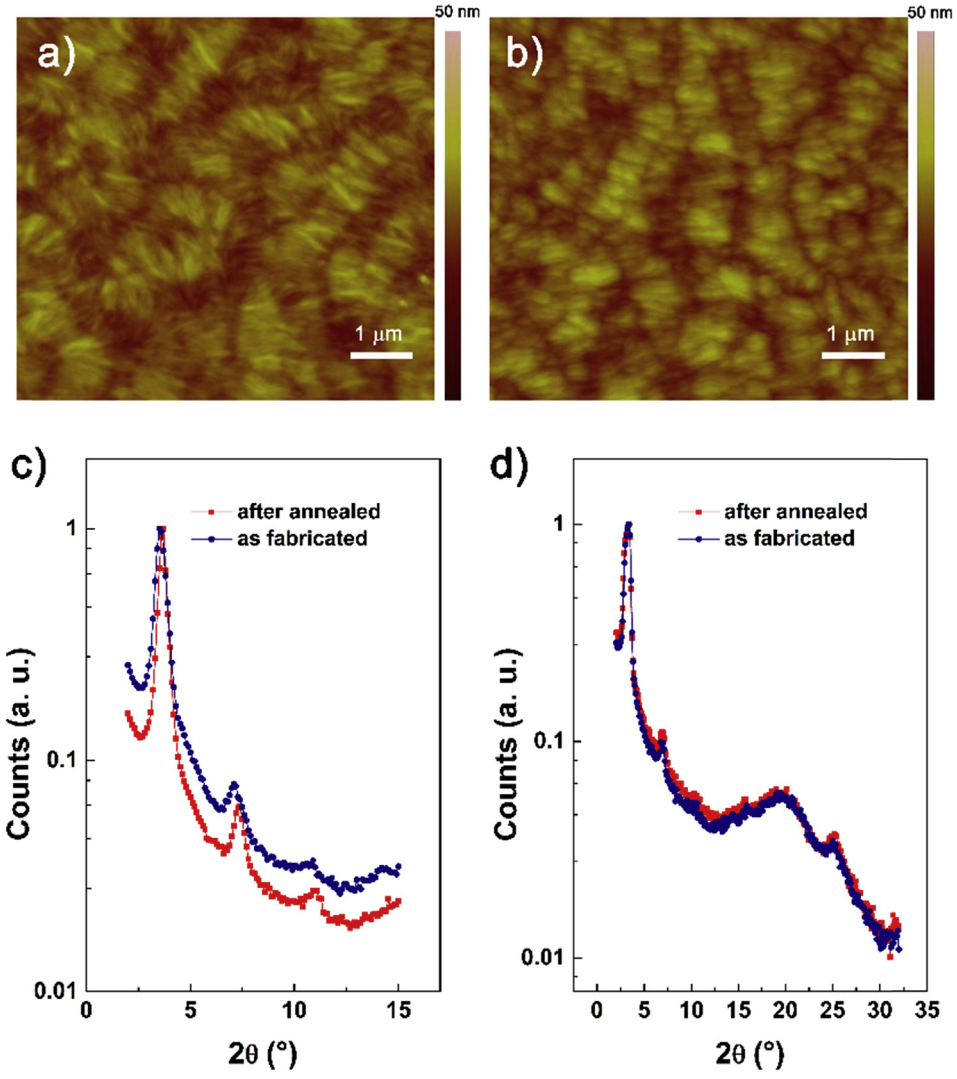

Fig. 5. AFM topography image of **P1** thin films: a) before annealing, b) after annealing at 120 °C. GXRD patterns of the **P1** thin films before and after annealing at 120 °C. c) Out-of-plane, d) In-plane ($\lambda = 2dsin\theta = 1.54$ Å).

PFETs based on both copolymers exhibit promising device performances, indicating that the **NDTT** units are a kind of potential building blocks in constructing D–A semiconducting polymers for organic electronics.

Acknowledgments

This work was financially supported by the National Natural Science Foundation of China (21474116 and 51233006) and the Strategic Priority Research Program of the Chinese Academy of Sciences (XDB12030100). This work was also supported by GRF (HKBU 203212), Theme-Based Research Scheme (Project No. [T23-713/11]), Hong Kong Research Grants Council and Open Research Fund of State Key Laboratory of Polymer Physics and Chemistry, Changchun Institute of Applied Chemistry, Chinese Academy of Sciences. The GXRD tests were carried out at 1W1A station of Beijing Synchrotron Radiation Facility (BSRF), BL16B1 Station of Shanghai Synchrotron Radiation Facility (SSRF), and 23A1 Station of National Synchrotron Radiation Research Centre (NSRRC, Taiwan). The authors gratefully thank the assistance of scientists from the stations during the experiments.

Appendix A. Supplementary data

Supplementary data related to this article can be found at http://dx.doi.org/10.1016/j.dyepig.2016.03.048.

References

[1] (a) Thompson BC, Fréchet JMJ. Polymer-fullerene composite solar cells. Angew Chem Int Ed 2008;47:58–77.
(b) Brabec CJ, Gowrisanker S, Halls JJM, Laird D, Jia S, Williams SP. Polymer–fullerene bulk-heterojunction solar cells. Adv Mater 2010;22:3839–56.

[2] (a) Wang CL, Dong HL, Hu WP, Liu YQ, Zhu DB. Semiconducting π-conjugated systems in field-effect transistors: a material odyssey of organic electronics. Chem Rev 2012;112:2208–67.
(b) Zhang WF, Liu YQ, Yu G. Heteroatom substituted organic/polymeric semiconductors and their applications in field-effect transistors. Adv Mater 2014;26:6898–904.

[3] (a) Wang EG, Ma Z, Zhang Z, Vandewal K, Henriksson P, Ingans O, et al. An easily accessible isoindigo-based polymer for high-performance polymer solar cells. J Am Chem Soc 2011;133:14244–7.
(b) Osaka I, Kakara T, Takemura N, Koganezawa T, Takimiya K. Naphthodithiophene-naphthobisthiadiazole copolymers for solar cells: alkylation drives the polymer backbone flat and promotes efficiency. J Am Chem Soc 2013;135:8834–7.

[4] Zhan XW, Tan ZA, Domercq B, An ZS, Zhang X, Barlow S, et al. A high-mobility electron-transport polymer with broad absorption and its use in field-effect transistors and all-polymer solar cells. J Am Chem Soc 2007;129:7246–7.

[5] Shi SW, Xie XD, Gao C, Shi KL, Chen S, Yu G, et al. Synthesis and characterization of angular-shaped naphtho[1,2-*b*;5,6-*b*′]difuran-diketopyrrolopyrrole-containing copolymers for high-performance organic field-effect transistors. Macromolecules 2014;47:616–25.

[6] (a) Lei T, Cao XY, Fan Y, Liu CJ, Yuan SC, Pei J. High-performance air-stable organic field-effect transistors: isoindigo-based conjugated polymers. J Am Chem Soc 2011;133:6099–101.
(b) Koizumi Y, Ide M, Saeki A, Vijayakumar C, Balan B, Kawamotoa M, et al. Thienoisoindigo-based low-band gap polymers for organic electronic devices. Polym Chem 2013;4:484–94.

[7] He ZC, Zhong CM, Su SJ, Xu M, Wu HB, et al. Enhanced power-conversion efficiency in polymer solar cells using an inverted device structure. Nat Phot 2012;6:591–5.

[8] Peng Q, Liu XJ, Su D, Fu GW, Xu J, Dai LM, et al. Novel benzo[1,2-*b*:4,5-*b*′]dithiophene-benzothiadiazole derivatives with variable side chains for high-performance solar cells. Adv Mater 2011;23:4554–8.

[9] Qian DP, Ye L, Zhang MJ, Liang YR, Li LJ, Huang Y, et al. Design, application, and morphology study of a new photovoltaic polymer with strong aggregation in solution state. Macromolecules 2012;45:9611–7.

[10] (a) Chen JD, Cui C, Li YQ, Zhou L, Ou QD, Li C, et al. Single-junction polymer solar cells exceeding 10% power conversion efficiency. Adv Mater 2015;27:1035–41.
(b) Lia SH, Jhuo HJ, Yeh PN, Cheng YS, Li YL, Lee YH, et al. Single junction inverted polymer solar cell reaching power conversion efficiency 10.31% by employing dual-doped zinc oxide nano-film as cathode interlayer. Sci Rep 2014;4:6813.

[11] (a) Chen HJ, Guo YL, Yu G, Zhao Y, Zhang J, Gao D, et al. Highly π-extended copolymers with diketopyrrolopyrrole moieties for high-performance field-effect transistors. Adv Mater 2012;24:4618–22.
(b) Kang I, Yun HJ, Chung DS, Kwon SK, Kim YH. Record high hole mobility in polymer semiconductors via side chain engineering. J Am Chem Soc 2013;135:14896–9.
(c) Li J, Zhao Y, Tan HS, Guo YL, Di CA, Yu G, et al. A stable solution-processed polymer semiconductor with record high-mobility for printed transistors. Sci Rep 2012;2:754.

[12] (a) Tseng HR, Phan H, Luo C, Wang M, Perez LA, Patel SN, et al. High-mobility field-effect transistors fabricated with macroscopic aligned semiconducting polymers. Adv Mater 2014;26:2993–8.
(b) Lei T, Dou JH, Cao XY, Wang JY, Pei J. Electron-deficient poly(*p*-phenylene vinylene) provides electron mobility over 1 $cm^2 V^{-1} s^{-1}$ under ambient conditions. J Am Chem Soc 2013;135:12168–71.

[13] Osaka I, Abe T, Shinamura S, Takimiya K. Impact of isomeric structures on transistor performances in naphthodithiophene semiconducting polymers. J Am Chem Soc 2011;133:6852–60.

[14] Osaka I, Abe T, Shinamura S, Miyazaki E, Takimiya K. High-mobility semiconducting naphthodithiophene copolymers. J Am Chem Soc 2010;132:5000–1.

[15] (a) Nketia-Yawson B, Lee HS, Seo D, Yoon Y, Park WT, Kwak K, et al. A highly planar fluorinated benzothiadiazole-based conjugated polymer for high-performance organic thin-film transistors. Adv Mater 2015;27:3045–52.
(b) Fu L, Fu W, Cheng P, Xie Z, Fan C, Shi M, et al. A diketopyrrolopyrrole molecule end-capped with a furan-2-carboxylate moiety: the planarity of molecular geometry and photovoltaic properties. J Mater Chem A 2014;2:6589–97.

[16] (a) He B, Pun AB, Klivansky LM, McGough A, Ye Y, Zhu J, et al. Thiophene fused azacoronenes: regioselective synthesis, self-organization, charge transport, and its incorporation in conjugated polymers. Chem Mater 2014;26:3920–7.
(b) He B, Dai J, Zherebetskyy D, Chen TL, Zhang BA, Teat SJ, et al. A divergent route to core- and peripherally functionalized diazacoronenes that act as colorimetric and fluorescence proton sensors. Chem Sci 2015;6:3180–6.
(c) He B, Zhang AB, Liu F, Navarro A, Fernández-Liencres MP, Lu R, et al. Electronic and morphological studies of conjugated polymers incorporating a disk-shaped polycyclic aromatic hydrocarbon unit. ACS Appl Mater Inter 2015;7:20034–45.

[17] (a) Wang B, Tsang SW, Zhang WF, Tao Y, Wong MS. Naphthodithiophene-2,1,3-benzothiadiazole copolymers for bulk heterojunction solar cells. Chem Commun 2011;47:9471–3.
(b) Wang B, Zhang J, Tam HL, Wu B, Zhang WF, Chan MS, et al. Impact of alkyl side chains on the photovoltaic and charge mobility properties of naphthodithiophene–benzothiadiazole copolymers. Polym Chem 2014;5:836–43.

[18] Yang LQ, Zhou H, You W. Quantitatively analyzing the influence of side chains on photovoltaic properties of polymer-fullerene solar cells. J Phys Chem C 2010;114:16793–800.

[19] Zhang J, Li ZG, Xing H, Zhang WF, Guo L, Liu YQ, et al. Naphthodithieno[3,2-*b*]thiophene-based semiconductors: synthesis, characterization, and device performance of field-effect transistors. Org Chem Front 2014;1:333–7.

[20] Stalder R, Mei JG, Subbiah J, Grand C, Estrada LA, So F. n-Type conjugated polyisoindigos. Macromolecules 2011;44:6303–10.

[21] Mahmood K, Liu ZP, Li CH, Lu Z, Fang T, Liu X, et al. Novel isoindigo-based conjugated polymers for solar cells and field effect transistors. Polym Chem 2013;4:3563–74.

[22] Ha JS, Kim KH, Choi DH. 2,5-Bis(2-octyldodecyl)pyrrolo[3,4-c]pyrrole-1,4-(2*H*,5*H*)-dione-based donor-acceptor alternating copolymer bearing 5′-di(thiophen -2-yl)-2,2-biselenophene exhibiting 1.5 $cm^2 V^{-1} s^{-1}$ hole mobility in thin-film transistors. J Am Chem Soc 2011;133:10364–7.

[23] Mao ZP, Zhang WF, Huang JY, Shi KL, Gao D, Chen ZH, et al. High-performance polymer field-effect transistors fabricated with low-bandgap DPP-based semiconducting materials. Polym Chem 2015;6:6457–64.

[24] Veldman D, İpek Ö, Meskers SCJ, Sweelssen J, Koetse MM, Veenstra SC, et al. Compositional and electric field dependence of the dissociation of charge transfer excitons in alternating polyfluorene copolymer/fullerene blends. J Am Chem Soc 2008;130:7721–35.

[25] Ortiz RP, Herrera H, Blanco RL, Huang H, Facchetti A, Marks TJ, et al. Organic n-channel field-effect transistors based on arylenediimide-thiophene derivatives. J Am Chem Soc 2010;132:8440–52.

[26] Tsao HN, Cho DM, Park I, Hansen MR, Mavrinskiy A, Yoon DY, et al. Ultrahigh mobility in polymer field-effect transistors by design. J Am Chem Soc 2011;133:2605–12.

View publication stats